



Modelling of biodiesel fuel droplet heating and evaporation: Effects of fuel composition



M. Al Qubeissi, S.S. Sazhin^{*}, C. Crua, J. Turner, M.R. Heikal

Sir Harry Ricardo Laboratories, Centre for Automotive Engineering, School of Computing, Engineering and Mathematics, Faculty of Science and Engineering, University of Brighton, Brighton BN2 4GJ, UK

HIGHLIGHTS

- Discrete Components Model taking into account liquid species diffusion.
- A comparative analysis of time evolutions of droplet surface temperatures and radii.
- Various types of biodiesel fuels.

ARTICLE INFO

Article history:

Received 22 January 2015

Received in revised form 16 March 2015

Accepted 18 March 2015

Available online 28 March 2015

Keywords:

Biodiesel fuel

Methyl esters

Multi-component droplets

Heating

Evaporation

Modelling

ABSTRACT

A comparative analysis of predictions of several models of biodiesel fuel droplet heating and evaporation in realistic Diesel engine-like conditions is presented. Nineteen types of biodiesel fuels composed of methyl esters are used for the analysis. It is shown that the model, based on the assumption that the diffusivity of species in droplets is infinitely fast and the liquid thermal conductivity is infinitely large, under-predicts the droplet evaporation time compared with the model taking into account the effects of finite diffusivity and conductivity, by up to about 15%. A similar under-predictions of the model in which the transient diffusion of species is ignored and the liquid thermal conductivity is assumed to be infinitely large, is shown to be about 26%. The latter result is not consistent with the earlier finding, based on the analysis of only five types of biodiesel fuels and different input parameters, in which it was shown that the deviations between the evaporation times predicted by these models do not exceed about 5.5%. As in the case of Diesel and gasoline fuel droplets, for biodiesel droplets the multi-component models predict higher droplet surface temperatures at the final stages of droplet evaporation and longer evaporation times than for the single-component models. This is related to the fact that at the final stages of droplet evaporation the mass fraction of heavier species, which evaporate more slowly than the lighter species and have higher boiling temperatures, increases at the expense of lighter species.

© 2015 Elsevier Ltd. All rights reserved.

1. Introduction

The interest to biodiesel fuels has been mainly stimulated by depletion of fossil fuels and the need to reduce carbon dioxide emissions that contribute toward climate change [1]. The term 'biodiesel' typically refers to "a fuel comprised of mono-alkyl esters of long-chain fatty acids derived from vegetable oils or animal fats" [2]. Biodiesel fuel is typically produced by chemical conversion of animal fats or vegetable oils [3,4]. The use of biodiesel fuel is expected to contribute to the reduction of global warming [5]. Also, using biodiesel fuel as an alternative to conventional fuels has a number of other advantages: it readily mixes with fossil

Diesel fuels, it is less polluting, has higher lubricity, higher flash point, it is cost effective, and can be used in Diesel engines with minimal modifications [6–9]. According to the U.S. Environmental Protection Agency – Tier I and Tier II standards (see [10] for details), currently produced biodiesel types have passed the health effects testing requirements [11].

The analysis presented in this paper is focused on the modelling of biodiesel fuel droplet heating and evaporation, which is an important stage of the process leading from the injection of biodiesel fuel into combustion chamber to its ultimate combustion, producing the driving force for internal combustion engines. In contrast to most previously suggested models for these processes, the temperature gradients and species diffusion inside droplets are taken into account based on the analytical solutions to heat transfer and species diffusion equations, which are incorporated into a

^{*} Corresponding author.

E-mail address: S.Sazhin@brighton.ac.uk (S.S. Sazhin).

Table 1

Types of biodiesel fuels, their abbreviations, acid codes and molar fractions of the components (pure methyl esters). Symbols 'M' for the acid codes are omitted.

Methyl esters	Abbreviations	Fatty acids																	
		C8:0	C10:0	C12:0	C14:0	C16:0	C17:0	C18:0	C20:0	C22:0	C24:0	C16:1	C18:1	C20:1	C22:1	C24:1	C18:2	C18:3	Others
Tallow	TME	–	–	0.20	2.50	27.90	–	23.00	0.40	0.40	–	2.50	40.00	0.30	0.30	–	2.00	–	0.50
Lard	LME	–	–	–	1.00	26.00	–	14.00	–	–	–	2.80	44.00	2.00	2.00	–	8.00	–	0.20
Butter	BME	5.19	2.80	3.40	10.99	31.66	–	10.79	0.40	0.40	–	2.40	26.37	1.00	1.00	–	3.00	0.60	–
Coconut	CME	6.00	8.00	50.00	15.00	9.00	–	3.00	–	–	–	–	7.00	–	–	–	2.00	–	–
Palm Kernel	PMK	2.60	4.00	50.00	17.00	8.00	–	1.70	1.50	1.50	–	0.40	12.00	–	–	–	1.30	–	–
Palm	PME	–	–	0.26	1.29	45.13	–	4.47	0.35	0.17	–	0.21	38.39	–	–	–	9.16	0.19	0.38
Safflower	SFE	–	–	–	–	5.20	–	2.20	–	–	–	–	76.38	–	–	–	16.22	–	–
Peanut	PTE	–	–	–	0.50	8.00	–	4.00	7.00	7.00	–	1.50	49.00	–	–	–	23.00	–	–
Cottonseed	CSE	–	–	–	2.00	19.00	–	2.00	–	–	–	–	31.00	2.50	2.50	–	41.00	–	–
Corn	CNE	–	–	–	1.00	9.00	–	2.50	–	–	–	1.50	40.00	1.00	1.00	–	44.00	–	–
Sunflower	SNE	–	–	–	–	5.92	–	4.15	1.38	1.38	–	–	18.46	–	–	–	68.41	0.30	–
Tung	TGE	–	–	–	–	3.64	–	2.55	–	13.14	–	–	10.10	0.81	–	–	13.75	51.64	4.37
Hemp1	HME1	–	–	–	–	6.62	0.21	2.06	0.45	0.25	0.23	0.33	11.88	0.27	0.17	0.15	56.71	20.67	–
Soybean	SME	–	–	–	0.30	10.90	–	4.40	0.40	–	–	–	24.00	–	–	–	52.80	7.20	–
Linseed	LNE	–	–	–	0.20	6.20	–	0.60	–	–	–	–	18.00	–	–	–	16.00	59.00	–
Hemp2	HME2	–	–	–	–	6.51	–	2.46	0.90	–	–	–	11.88	0.90	–	–	54.82	20.07	2.46
Canola seed	CAN	–	–	–	–	4.48	0.14	1.99	0.62	0.35	0.16	0.36	59.66	1.49	0.42	–	20.89	9.44	–
Waste oil	WME	–	–	0.20	0.67	15.69	0.20	6.14	0.39	0.44	0.30	0.73	42.84	0.56	0.15	–	29.36	2.03	0.30
Rapeseed	RME	–	–	–	–	4.93	–	1.66	0.56	–	–	–	26.61	–	22.32	0.77	24.75	9.70	8.70

Table 2

Names, acid codes, molecular formulae, molar masses and boiling points of the components (pure methyl esters) presented in Table 1.

Fatty acids	Acid code	Molecular formula	Molar mass (g/mol)	Boiling Point (K)
Methyl octanoate	C8:0M	C ₉ H ₁₈ O ₂	144.212	467.5
Methyl decanoate	C10:0M	C ₁₁ H ₂₂ O ₂	172.265	501.1
Methyl dodecanoate	C12:0M	C ₁₃ H ₂₆ O ₂	214.338	530.42
Methyl tetradecanoate	C14:0M	C ₁₅ H ₃₀ O ₂	242.39	554.20
Methyl palmitate	C16:0M	C ₁₇ H ₃₄ O ₂	270.442	577.98
Methyl heptadecanoate	C17:0M	C ₁₈ H ₃₆ O ₂	284.468	589.87
Methyl stearate	C18:0M	C ₁₉ H ₃₈ O ₂	298.494	601.76
Methyl eicosanoate	C20:0M	C ₂₁ H ₄₂ O ₂	326.546	625.55
Methyl docosanoate	C22:0M	C ₂₃ H ₄₆ O ₂	354.598	649.33
Methyl tetracosanoate	C24:0M	C ₂₅ H ₅₀ O ₂	382.65	673.11
Methyl palmitoleate	C16:1M	C ₁₇ H ₃₂ O ₂	268.426	577.57
Methyl oleate	C18:1M	C ₁₉ H ₃₆ O ₂	296.478	601.31
Methyl eicosenoate	C20:1M	C ₂₁ H ₄₀ O ₂	324.53	625.05
Methyl erucate	C22:1M	C ₂₃ H ₄₄ O ₂	352.582	648.79
Methyl nervonate	C24:1M	C ₂₅ H ₄₈ O ₂	380.634	672.53
Methyl linoleate	C18:2M	C ₁₉ H ₃₄ O ₂	294.462	601.3
Methyl linolenate	C18:3M	C ₁₉ H ₃₂ O ₂	292.446	601.58
Others	–	–	296.478	601.31

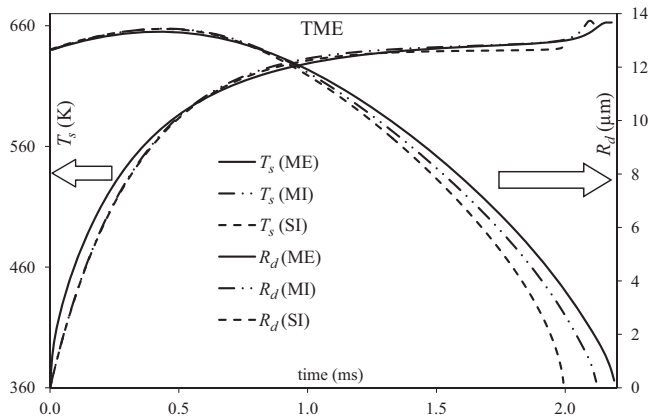


Fig. 1. The plots of time evolution of droplet's surface temperature (T_s) and radius (R_d) for Tallow Methyl Ester (TME) predicted by the multi-component ETC/ED model (ME), single-component (zero diffusivity)/ITC model (SI), and multi-component ITC/ID model (MI). The droplet is assumed to have initial radius 12.66 μm and is moving at 28 m/s in still air at temperature and pressure equal to 700 K and 3.2 MPa respectively.

numerical algorithm [12]. Unlike typical fossil fuels, such as gasoline and Diesel fuels, which are composed of hundreds of components, biodiesel fuel is composed of a relatively small (6–14) number of fatty acid ethyl and methyl esters [13–16] (only biodiesels composed of methyl esters will be studied in our paper). This allows us to analyse species diffusion inside droplets based on the Discrete Component Model (DCM) in which the diffusion of species is described without any additional approximations (cf. the analysis of Diesel fuel droplet heating and evaporation described in [17]).

The preliminary results of modelling biodiesel fuel droplet heating and evaporation, using the abovementioned approach, were presented in [18]. The analysis of that paper was based on only five types of biodiesel fuel and it was concluded that the predictions of the multi-component and single-component (when the contribution of all components was approximated by the contribution of a single component with averaged characteristics) models are rather close (the droplet evaporation times predicted by these models differed by less than about 5.5% for typical Diesel engine-like conditions).

In the current paper, the analysis, similar to the one presented in [18], is performed but for a much wider range of biodiesel fuels

(19 types altogether) and more realistic engine conditions. Since our analysis is based on a rather wide selection of biodiesel fuels the relevance of the results to practical engineering applications is expected to be more credible compared with the results presented in [18]. Also, they will allow us to get clearer idea about the effect of composition on biodiesel fuel droplet heating and evaporation.

The compositions of biodiesel fuel, used in our analysis are presented in Section 2. The main features of the model and numerical algorithm are summarised in Section 3. The input parameters used in the calculations are summarised in Section 4. The results of our calculations are presented and discussed in Section 5. The main results of the paper are summarised in Section 6.

2. Compositions of biodiesel fuels

The following types of biodiesel fuel are used in our analysis: Tallow Methyl Ester (TME), Lard Methyl Ester (LME), Butter Methyl Ester (BME), Coconut Methyl Ester (CME), Palm Kernel Methyl Ester (PMK), Palm Methyl Ester (PME), Safflower Methyl Ester (SFE), Peanut Methyl Ester (PTE), Cottonseed Methyl Ester (CSE), Corn Methyl Ester (CNE), Sunflower Methyl Ester (SNE), Tung Methyl Ester (TGE), Hemp-oil Methyl Ester, produced from Hemp seed oil in Ukraine (HME1), Soybean Methyl Ester (SME), Linseed Methyl Ester (LNE), Hemp-oil Methyl Ester, produced in European Union (HME2), Canola seed Methyl Ester (CAN), Waste

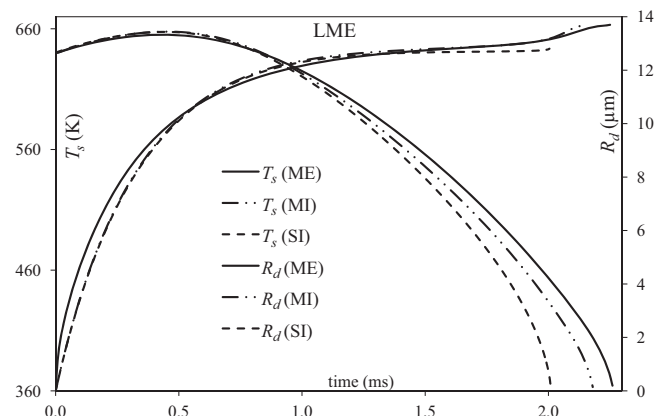


Fig. 2. The same as Fig. 1 but for a Lard Methyl Ester (LME) droplet.

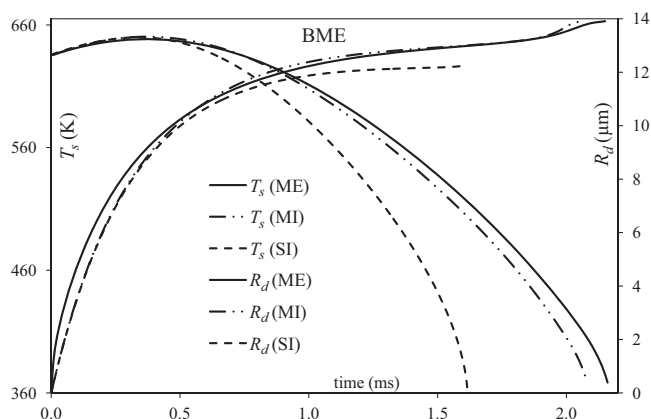


Fig. 3. The same as Figs. 1 and 2, but for a Butter Methyl Ester (BME) droplet.

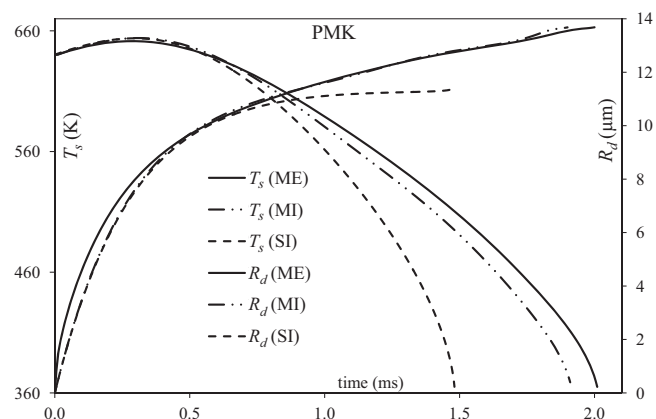


Fig. 5. The same as Figs. 1–4, but for a Palm Kernel Methyl Ester (PMK) droplet.

cooking-oil Methyl Ester (WME) and Rapeseed Methyl Ester (RME). The molar fractions of the components of these fuels (in percent), inferred from averaging data presented in [4,19–24], are shown in Table 1.

The meaning of symbols of components, presented in Table 1, and their acid codes, molecular formulae, molar masses and boiling temperatures are shown in Table 2 (the values of boiling temperatures in this table are taken from [25,18]). The symbols of components in Tables 1 and 2 show the numbers of carbon atoms in fatty acids (nacid) and numbers of double bonds (DB). For example, C18:1M has nacid = 18 and DB = 1. The addition of one more carbon atom gives the total number of carbon atoms in methyl esters (nacid + 1). There are other names used for some methyl esters shown in Table 2. For example, 'Methyl dodecanoate' is also known as 'Methyl laurate', 'Methyl tetradecanoate' is also known as 'Methyl myristate' and 'Methyl docosanoate' is also known as 'Methyl behenate' (see [18,26,27] for the details).

The molar fractions of unidentified additives in biodiesel fuels vary from 0 to around 8.7%, and is shown in Table 1 as 'Others'. Since the exact nature of these components has not been identified, there is a certain freedom in selecting their transport and thermodynamic properties. In [18] we calculated these properties as the arithmetic weighted averages of the corresponding values for all remaining components (C12:0M to C18:3M in the case considered in [18]). In the present study we assume that these properties are identical to those of C18:1M. The properties computed using this assumption turned out to be close to those obtained in [18], but the calculations are much simpler as they do not require

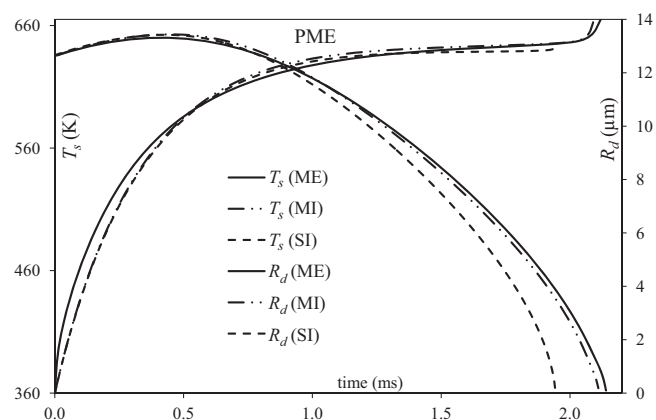


Fig. 6. The same as Figs. 1–5, but for a Palm Methyl Ester (PME) droplet.

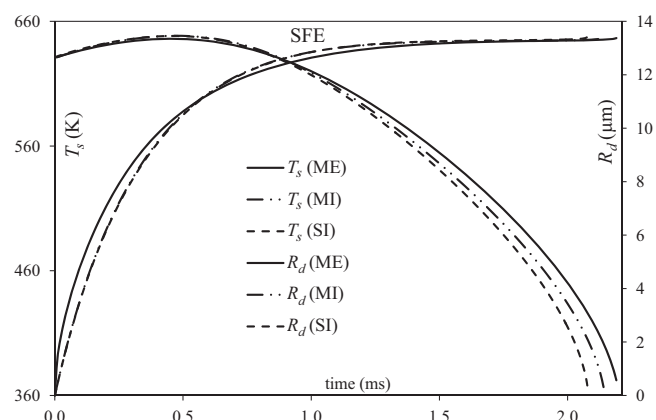


Fig. 7. The same as Figs. 1–6, but for a Safflower Methyl Ester (SFE) droplet.

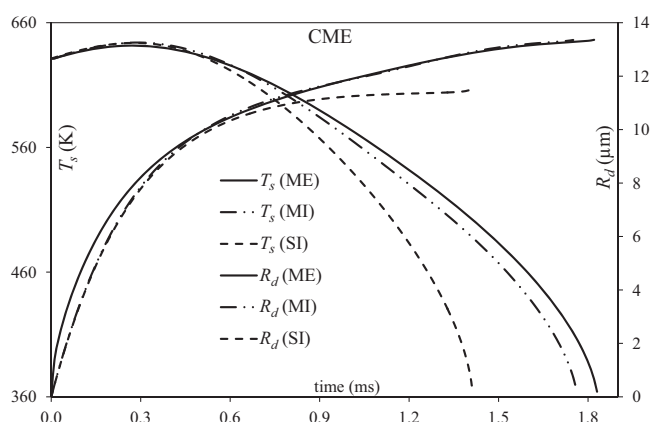


Fig. 4. The same as Figs. 1–3, but for a Coconut Methyl Ester (CME) droplet.

an averaging procedure. Only 3 fuels have non-negligible molar fractions of unidentified components: RME, TGE, and HME2. The molar fractions of unidentified components in other biodiesel fuels are either negligible or non-existent (see Table 1).

The transport and thermodynamic properties of all components shown in Tables 1 and 2 are given in Appendix B of [18]. These properties were extrapolated to the cases of other fatty acids shown in Table 2, which have not been considered in [18].

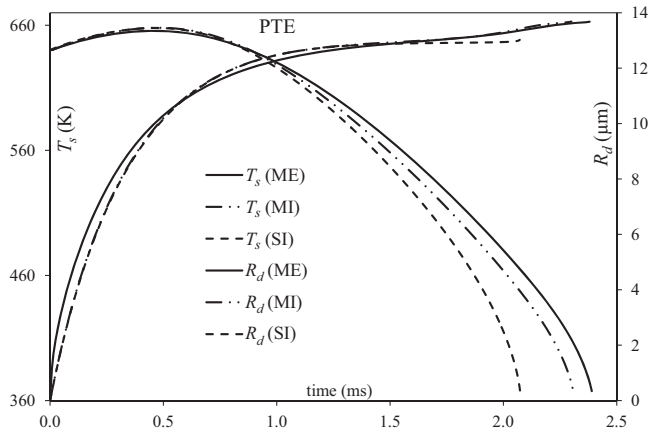


Fig. 8. The same as Figs. 1–7, but for a Peanut Methyl Ester (PTE) droplet.

3. The model and numerical algorithm

The model and numerical algorithm used in our analysis are exactly the same as the ones used in [18]. The model takes into account the effects of multi-component droplet heating by convection, its evaporation, the finite thermal conductivity, recirculation, and species diffusion in the liquid phase. Only the effects of ambient gas on droplets are taken into account.

The predictions of the following models are compared:

- (1) a model taking into account the contributions of all components of biodiesel fuels, their realistic diffusion (see [18] for the details), temperature gradient, and recirculation within the droplet, in the case of moving droplets (using the Effective Thermal Conductivity/Effective Diffusivity (ETC/ED) model); this model is referred to as the 'ME' model;
- (2) a model taking into account the contribution of all components of biodiesel fuels, but assuming that the diffusivity of species in droplets is infinitely fast and the liquid thermal conductivity is infinitely large (using the Infinite Thermal Conductivity/Infinite Diffusivity (ITC/ID) model); this model is referred to as the 'MI' model;
- (3) a model ignoring transient diffusion of species (treating all species as a single component with properties depending only on temperature, which was updated at each time step) and assuming that the liquid thermal conductivity is infinitely large (ITC model); this model is referred to as the 'SI' model. In the case of stationary droplets this model is further

simplified assuming that biodiesel fuels can be approximated by a single dominant (with the largest molar fraction) component. The latter model is referred to as the 'DI' model.

4. Input parameters

As in [18], the initial droplet radius is assumed equal to $R_{d0} = 12.66 \mu\text{m}$, which falls within the ranges reported in [28–31]. A droplet of initial temperature $T_{d0} = 360 \text{ K}$ is assumed to be moving through air at constant velocity of $U_d = 28 \text{ m/s}$. In the case of Butter Methyl Ester (BME) the calculations have also been performed for stationary droplets. Ambient temperature and pressure are assumed equal to 700 K and 3.2 MPa respectively. The droplet velocity was derived from the microscopic panorama images of Diesel spray interface [32,33] based on the assumption that biodiesel and Diesel fuel droplets move at approximately the same velocities under the same ambient conditions.

5. Results and discussions

The plots of time evolution of droplet surface temperature (T_s) and radius (R_d) for Tallow Methyl Ester (TME) are shown in Fig. 1. The general trends of the curves shown in this figure are the same as presented in the previous paper [18]. The ME model predicts longer evaporation times compared with the MI and SI models with the results predicted by the MI model being closer to those predicted by the ME model compared to the predictions of the SI model. The relative error in the evaporation times predicted by the SI model compared with the ME model is 9.0%. The same error for the MI model is 3.2%. That means that predictions of the models based on the assumption that species inside droplets mix infinitely fast are more reliable than the predictions of the models approximating TME by a single component. The MI model is one of the most widely used models for the analysis of heating and evaporation of complex hydrocarbon fuel mixtures (see, for example, Refs. [34–39]). The deviations between the predictions of SI and ME models are larger than those reported in [18] (5.5%). Note that both MI and ME models predict higher droplet surface temperatures at the final stages of droplet evaporation than the single-component model (SI). This is related to the fact that at the final stages of droplet evaporation the mass fraction of heavier species increases at the expense of lighter species. The heavier species evaporate more slowly than the lighter species and have higher boiling temperatures (see the results shown later in this paper). The same behaviour of temperatures is observed for other types of biodiesel fuel discussed below.

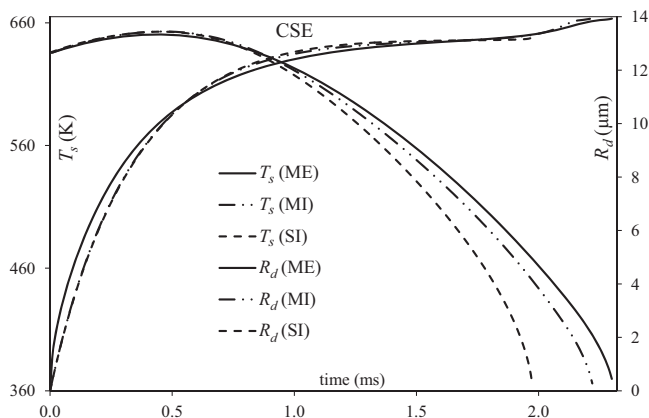


Fig. 9. The same as Figs. 1–8, but for a Cottonseed Methyl Ester (CSE) droplet.

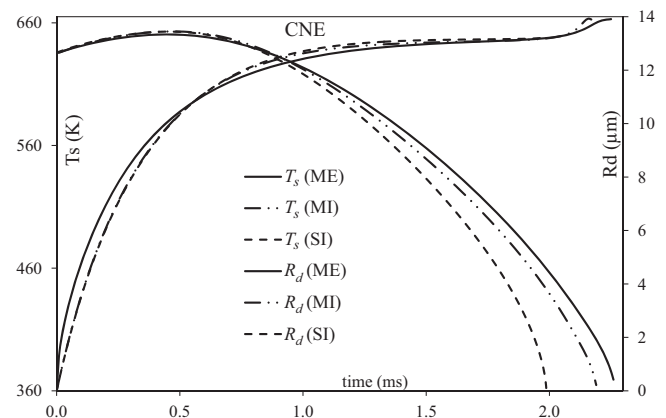


Fig. 10. The same as Figs. 1–9, but for a Corn Methyl Ester (CNE) droplet.

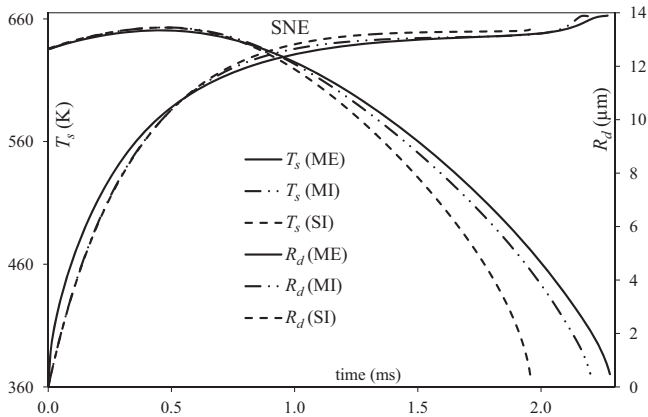


Fig. 11. The same as Figs. 1–10, but for a Sunflower Methyl Ester (SNE) droplet.

The same plots as shown in Fig. 1, but for Lard Methyl Ester (LME) are shown in Fig. 2. The curves shown in Fig. 2 are similar to those shown in Fig. 1. As in the case of TME, the results predicted by the MI model are closer to those predicted by the ME model compared with the predictions of the SI model. The relative errors in the evaporation times predicted by the SI and MI models compared with the ME model are slightly larger for LME compared with TME. These errors for the SI and MI models are found to be 11.1% and 4.0%, respectively.

The same plots as shown in Figs. 1 and 2, but for Butter Methyl Ester (BME) are presented in Fig. 3. The trends of the curves presented in Fig. 3 are similar to those shown in Figs. 1 and 2, but the relative error in the evaporation times predicted by the SI model compared with the ME model is much larger for BME compared with TME and LME. This error for the SI model was found to be 25.2%. The importance of this result lies in the fact that it contradicts one of the main conclusions made in our previous paper [18], based on the analysis of Palm Methyl Ester, Hemp Methyl Esters, Rapeseed oil Methyl Ester, and Soybean oil Methyl Ester. In [18] it was concluded that the droplet evaporation times predicted by the SI model differ by less than about 5.5% (note that the analysis of [18] was based on different values of input parameters compared with the current paper, except the initial droplet radii; the parameters used in [18] were obtained as average parameters described in the literature, while the parameters used in the current paper are inferred from in-house experimental data). This allowed the authors of [18] to conclude that if these errors can be tolerated, then biodiesel fuels can be safely approximated by single component fuels. The error of estimating the evaporation

time using the MI model, compared with the ME model, is found to be 3.7%. This is comparable with the results found for TME and LME.

The same plots as shown in Figs. 1–3, but for Coconut Methyl Ester (CME) and Palm Kernel Methyl Ester (PMK) are presented in Figs. 4 and 5 respectively. The shapes of the curves presented in these figures are rather similar to those shown in Fig. 3. The errors of estimating the evaporation times using the SI model, compared with the ME model, for CME and PMK are found to be 23.0% and 26.3% respectively. Similar errors but for the MI model are found to be 3.8% and 5.0% respectively. The latter errors are comparable with those shown in Figs. 1–3. Large errors of the estimations of the evaporation times for CME and PMK, using the SI model, reinforce the conclusion made based on the analysis of BME that the SI model cannot be used for the analysis of biodiesel droplet heating and evaporation unless errors of about 26% in predicted droplet evaporation times can be tolerated.

The shapes of the curves for time evolution of droplet surface temperature and radius, presented in Figs. 6 and 7 for Palm Methyl Ester (PME) and Safflower Methyl Ester (SFE), are similar to those shown in Figs. 1 and 2. As one can see from Figs. 6 and 7, the evaporation times predicted by the SI model for PME and SFE are less than those predicted by the ME model by 9.3% and 5.1% respectively. At the same time, using the MI model for PME and SFE leads to under-estimation of these times by 1.4% and 2.3% respectively. The curve $R_d(t)$ predicted by the MI model for PME is very close to the one predicted by the ME model, although the curves for droplet surface temperatures, predicted by both models are noticeably different.

The curves shown in Figs. 8–13 for Peanut Methyl Ester (PTE), Cottonseed Methyl Ester (CSE), Corn Methyl Ester (CNE), Sunflower Methyl Ester (SNE), Tung Methyl Ester (TGE) and Hemp Methyl Ester 1 (HME1) are reasonably close to those shown in Fig. 2. As one can see from these figures, the evaporation times predicted by the SI model for PTE, CSE, CNE, SNE, TGE and HME1 are less than those predicted by the ME model by 13.1%, 14.2%, 12.1%, 14.2%, 11.4% and 16.0% respectively. At the same time, using the MI model for PTE, CSE, CNE, SNE, TGE and HME1 leads to under-estimation of these times by 3.8%, 3.9%, 3.1%, 3.5%, 3.7% and 4.3% respectively.

The curves shown in Figs. 14–18 for Soybean Methyl Ester (SME), Linseed Methyl Ester (LNE), Hemp Methyl Ester 2 (HME2), Canola Seed Methyl Ester (CAN), and Waste oil Methyl Ester (WME) are reasonably close to those shown in Figs. 1 and 7. As one can see from these figures, the evaporation times predicted by the SI model for SME, LNE, HME2, CAN and WME are less than those predicted by the ME model by 4.1%, 3.5%, 4.0%, 6.8% and 8.7%

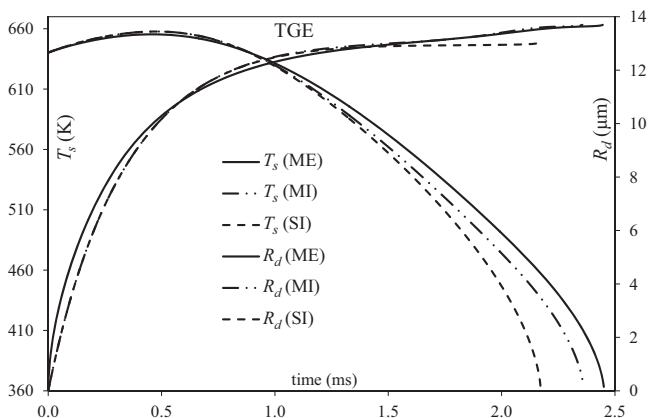


Fig. 12. The same as Figs. 1–11, but for a Tung Methyl Ester (TGE) droplet.

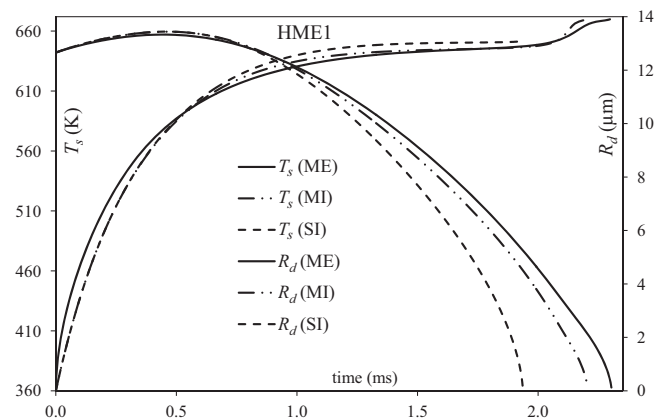


Fig. 13. The same as Figs. 1–12, but for a Hemp Methyl Ester 1 (HME1) droplet.

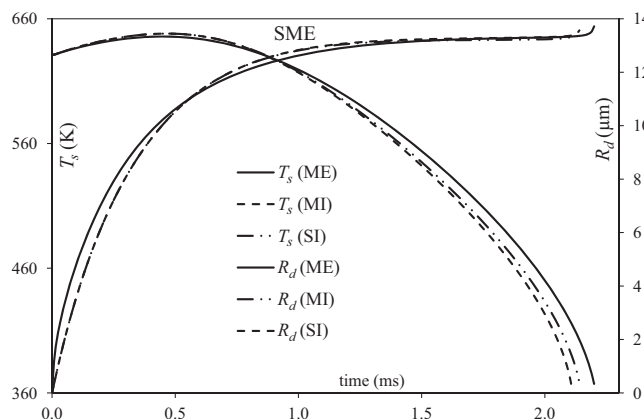


Fig. 14. The same as Figs. 1–13, but for a Soybean Methyl Ester (SME) droplet.

respectively. At the same time, using the MI model for SME, LNE, HME2, CAN and WME leads to under-estimation of these times by 2.7%, 2.1%, 2.8%, 3.7% and 3.9% respectively.

The curves shown in Fig. 19 for Rapeseed Methyl Ester (RME) are different from the ones shown in the previous figures due to the fact that both SI and MI models under-estimate considerably the droplet evaporation times, compared with the prediction of the ME model. These errors for the SI and MI models were found to be 18.4% and 15.1%, respectively. This shows that not only the SI model, but also the MI model can lead to considerable errors in estimating droplet evaporation times. Both models cannot be considered reliable for the analysis of droplet heating and evaporation unless errors of more than 15% can be tolerated. Note that the results shown in Fig. 19 are expected to be less reliable than the ones presented in other figures as RME contains the largest amount of additives the properties of which cannot be properly specified (with molar fraction 8.7%).

Note that the evaporation times shown in Figs. 1–19 cannot be directly compared with those shown in [18], as the latter were obtained for the values of parameters different from those used in the current paper. Also, the comparison so far has been focused mainly on the evaporation times, although the difference in the shapes of the curves T_s versus time predicted by various models is equally important for the assessment of the accuracy of the models. In all cases shown in Figs. 1–19 the ME model predicts higher droplet surface temperature at the initial stage of droplet heating and evaporation compared with the predictions of the MI and SI models (by about 7%). This is related to the fact that the ME model predicts that at the initial stage of droplet heating most of heat

supplied to the droplet is spent on heating the region close to the surface of the droplet (e.g. Fig. 22), while both SI and MI models are based on the assumption that the same heat is spread evenly over the whole volume of the droplet at any time. The behaviour of the temperature at intermediate times predicted by all models appears to be rather complex and is controlled by several competing factors including the rate of evaporation, heat transfer inside the droplet and heat supplied to the droplet. At the final stage of droplet evaporation, however, the surface temperature predicted by the ME and MI models becomes larger than the one predicted by the SI model. This can be related to the fact that at the final stage of droplet heating and evaporation, the ME and MI models predict that droplet composition is dominated by the heaviest component with the highest boiling temperature (see Table 2). The surface temperatures predicted by the ME and MI models at the final stages of droplet evaporation are rather similar as the droplet compositions predicted by both models at this stage of droplet evaporation are expected to be rather close. Note that predictions of temperatures by all models at the very final stage of droplet evaporation is not expected to be very reliable due to large time derivatives of droplet radii (see [40] for more detailed discussion of this phenomenon).

To provide a deeper understanding of the processes taking place during biodiesel fuel droplet heating and evaporation, in Figs. 20–22 we presented the plots of surface mass fractions of selected components versus time, the plots of mass fractions of selected components versus normalised distance from the droplet centre at various time instants and temperatures versus normalised distance from the droplet centre at various time instants for BME. The general shapes of these curves for other biodiesel fuels are similar to the ones for BME. All plots refer to the predictions of the ME model.

As follows from Fig. 20, the surface mass fractions of the lightest components (C8:0M, C12:0M and C14:0M) monotonically decrease with time. The surface mass fraction of the heaviest component (C22:1M) monotonically increases with time. The surface mass fractions of the intermediate components (C16:0M and C18:0M) first increase and then decrease with time. At the end of the evaporation process, only the heaviest and least volatile component remains at the droplet surface. This component is mainly responsible for prolonged droplet lifetime predicted by the ME model compared with the SI model, and higher surface temperatures at the final stage of droplet evaporation. The general shapes of the curves shown in Fig. 20 are similar to those predicted for other biodiesel fuels including the ones studied in our previous paper [18].

As one can see in Fig. 21, the decrease of the surface mass fraction of one of the lightest components (C12:0M) with time is

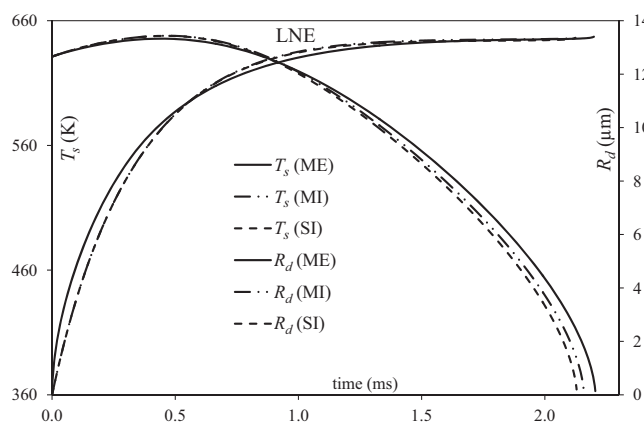


Fig. 15. The same as Figs. 1–14, but for a Linseed Methyl Ester (LNE) droplet.

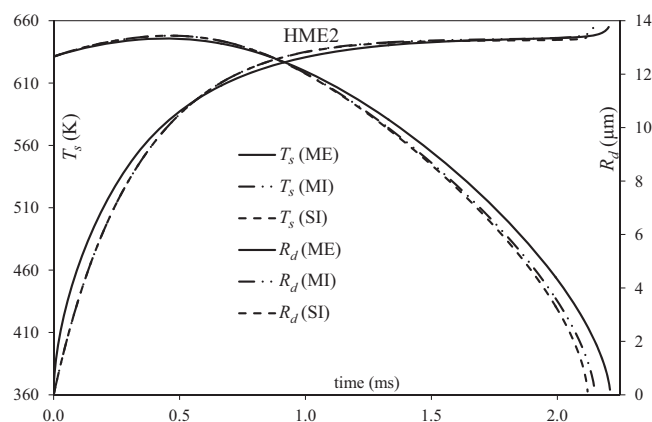


Fig. 16. The same as Figs. 1–15, but for a Hemp Methyl Ester 2 (HME2) droplet.

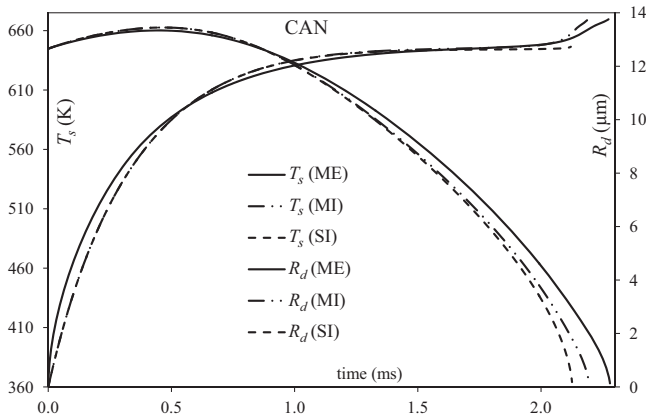


Fig. 17. The same as Figs. 1–16, but for a Canola Methyl Ester (CAN) droplet.

accompanied by the corresponding decrease of the mass fraction of this component in the body of the droplet. The rate of this decrease, however, reduces in the regions close to the droplet centre. Thus a negative gradient of this mass fraction is formed inside the droplet, which leads to the diffusion of this component from the droplet centre to its surface. As can be inferred from the same figure, the increase of the surface mass fraction of the heaviest components (C22:1M) with time is accompanied by the corresponding increase of the mass fraction of this component in the body of the droplet, although the rate of this increase reduces in the regions close to the droplet centre. Thus positive gradients of this mass fraction are formed inside the droplet, which lead to the diffusion of this component from the droplet surface to its centre. This leads to the formation of a droplet consisting mainly of the heaviest component (C22:1M) at the end of the evaporation process. One can clearly see from Fig. 21 that gradients of mass fractions of the components inside the droplet are initially small but increase with time. This observation shows the limitations of the well mixed models, including the MI model, widely used for the analysis of multi-component droplet heating and evaporation.

As one can see in Fig. 22, at the initial stage of droplet heating and evaporation (0.03 ms after the start of the process) rather large gradients of temperature inside the droplet close to droplet surface are formed. In contrast to the case of species molar fractions, however, the gradients of temperature inside droplets decrease with time. These gradients are reasonably small at 1 ms after the start of the process. This means that the Infinite Thermal Conductivity

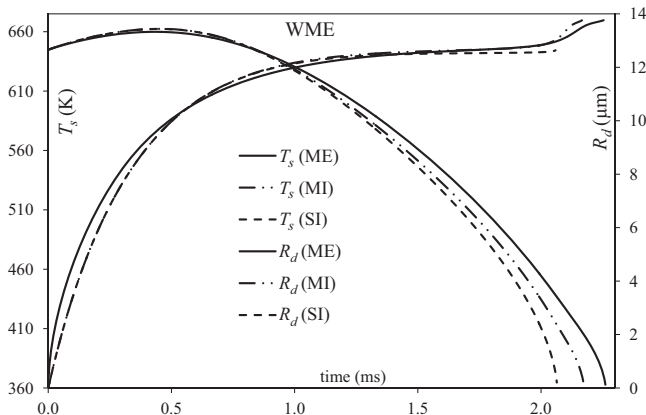


Fig. 18. The same as Figs. 1–17, but for a Waste Cooking Oil Methyl Ester (WME) droplet.

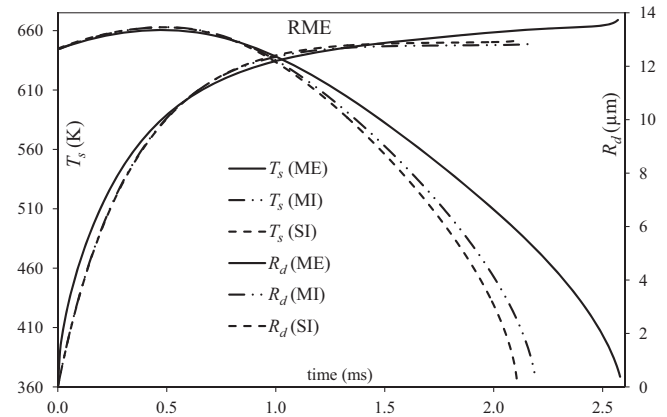


Fig. 19. The same as Figs. 1–18, but for a Rapeseed Methyl Ester (RME) droplet.

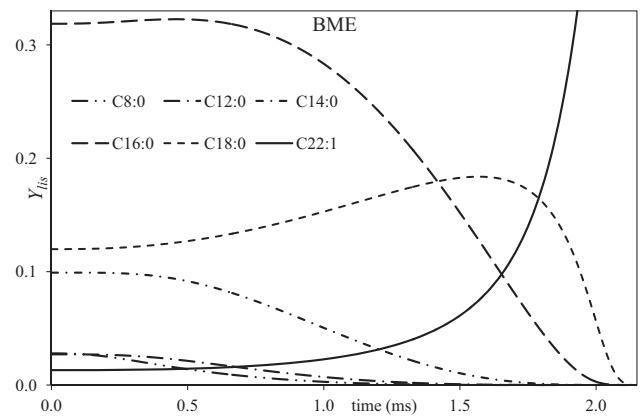


Fig. 20. The plots of time evolution of surface mass fractions of C8:0M, C12:0M, C14:0M, C16:0M, C18:0M and C22:1M for a Butter Methyl Ester (BME) droplet for the same conditions as in Figs. 1–19.

model can be applied to the analysis of droplet heating and evaporation, except at the very beginning of the process, when high accuracy of calculations is not required.

The plots of time evolution of droplet surface temperature (T_s) and radius (R_d) for BME at the same conditions as shown in Figs. 1–19 but for stationary droplets are shown in Fig. 23. The results predicted by the SI and ME models are shown, as in Fig. 3. Apart from these, the results predicted by the model based on the assumption that BME can be approximated by the dominant component (C16:0M) and assuming that the thermal conductivity of liquid is infinitely large are shown in the same figure (DI model). Note that in the case of stationary droplets the ME model reduces to the so called conduction limit model. In our case, however, the term 'ME model' is used for both stationary and moving droplets.

Comparing Figs. 3 and 23 one can see that moving droplets evaporate more than 5 times faster compared with the stationary droplets which can be attributed to increased Nusselt and Sherwood numbers of the moving droplets. At the same time the under-predictions of the evaporation times by the SI model compared with the ME model are about the same for moving (25.2%) and stationary (24.9%) droplets. The evaporation time predicted by the DI model turned out to be closer to the one predicted by the ME model than the evaporation time predicted by the SI model. The DI model under-predicted the evaporation time by 12.2%. This, however, is likely to be the case for this particular biodiesel fuel and cannot be generalised to other types of biodiesel fuels.

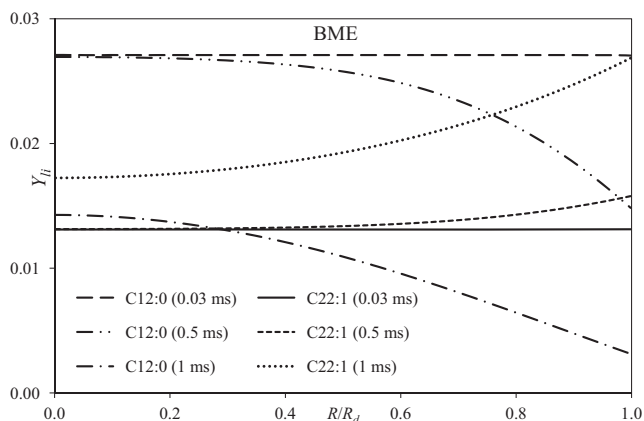


Fig. 21. The plots of mass fractions of C12:0M and C22:1M versus normalised distance from the droplet centre at three time instants 0.03 ms, 0.5 ms and 1 ms for a Butter Methyl Ester (BME) droplet for the same conditions as in Figs. 1–20.

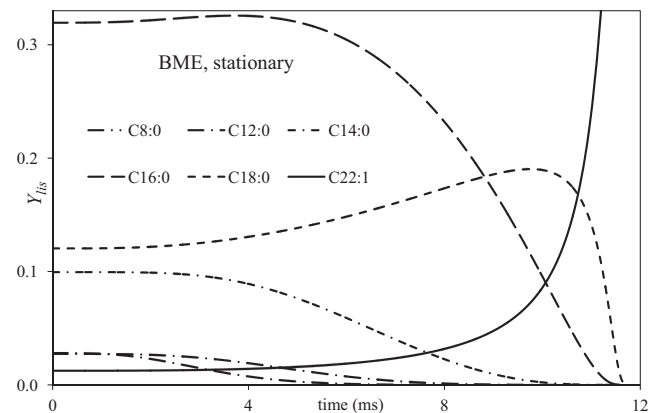


Fig. 24. The same as Fig. 20, but for a stationary Butter Methyl Ester (BME) droplet in the same conditions as in Fig. 23.

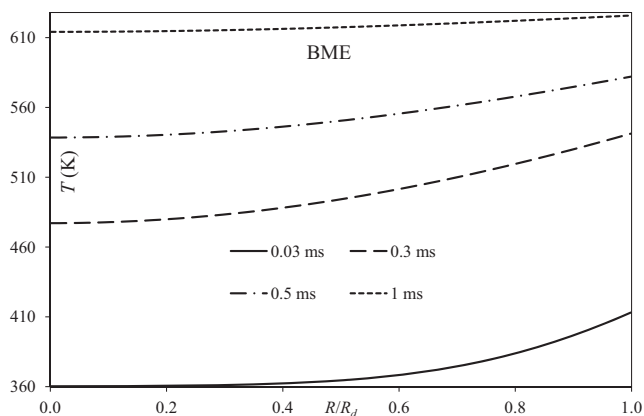


Fig. 22. The plots of temperature versus normalised distance from the droplet centre at four time instants 0.03 ms, 0.3 ms, 0.5 ms and 1 ms for a Butter Methyl Ester (BME) droplet for the same conditions as in Figs. 1–20.

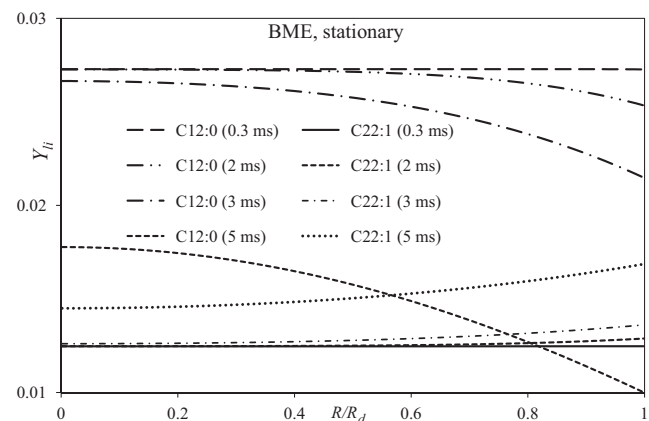


Fig. 25. The same as Fig. 21, but for a stationary Butter Methyl Ester (BME) droplet in the same conditions as in Fig. 23.

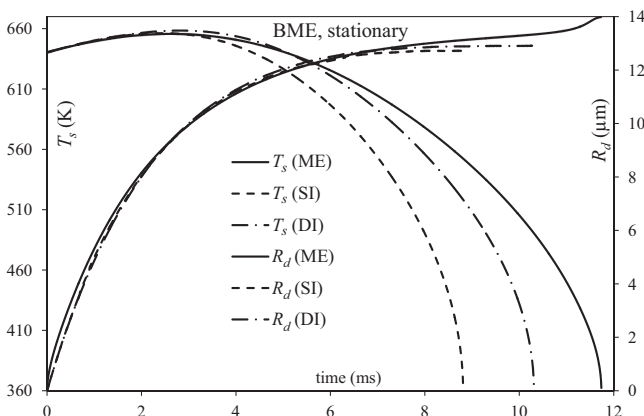


Fig. 23. The plots of time evolution of droplet's surface temperature (T_s) and radius (R_d) for Butter Methyl Ester (BME) predicted by the multi-component ETC/ED model (ME), single-component (zero diffusivity)/ITC model (SI), and a model in which BME is approximated by the dominant component C16:0M and using the assumption of infinite liquid thermal conductivity (DI). The droplet is assumed to be stationary in still air at temperature and pressure equal to 700 K and 3.2 MPa respectively; its initial radius is assumed equal to 12.66 μm.

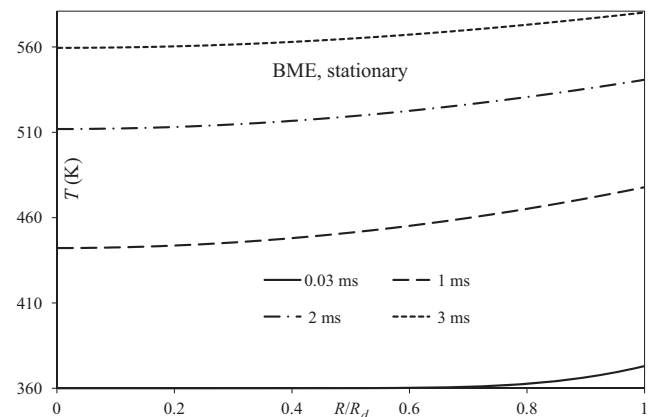


Fig. 26. The same as Fig. 22, but for a stationary Butter Methyl Ester (BME) droplet in the same conditions as in Fig. 23.

The plots similar to those shown in Figs. 20–22 but for stationary droplets are shown in Figs. 24–26. The main conclusions which can be inferred from the latter figures are the same as those inferred from Figs. 20–22. As one can see from Fig. 24, the light components are expected to be the first to evaporate and the heavy components are expected to be the last to evaporate. Gradients of mass fractions of components inside droplets increase with time, while the gradients of temperature inside droplets decrease with time. This shows that limitations of the MI and SI models widely used in the analysis of biodiesel fuel droplet heating and evaporation.

6. Conclusions

A comparative analysis of predictions of several models of biodiesel fuel droplet heating and evaporation in realistic Diesel engine-like conditions is presented. Firstly, a model taking into account the contributions of all components of biodiesel fuels, their realistic diffusion, temperature gradient, and recirculation within the droplet, in the case of moving droplets (Effective Thermal Conductivity/Effective Diffusivity (ETC/ED) model), is used. In the second model, the contribution of all components of biodiesel fuels are taken into account as in the first model, but the diffusivity of species in droplets is assumed to be infinitely fast and the liquid thermal conductivity is assumed to be infinitely large (Infinite Thermal Conductivity/Infinite Diffusivity (ITC/ID) model). In the third model, the transient diffusion of species is ignored and it is assumed that the liquid thermal conductivity is infinitely large. The fourth model is a simplified version of the third model in which it is assumed that biodiesel fuels can be approximated by a single dominant component (this model was used only for the analysis of stationary droplets).

Nineteen types of biodiesel fuel have been used in the analysis. These are Tallow Methyl Ester (TME), Lard Methyl Ester (LME), Butter Methyl Ester (BME), Coconut Methyl Ester (CME), Palm Kernel Methyl Ester (PMK), Palm Methyl Ester (PME), Safflower Methyl Ester (SFE), Peanut Methyl Ester (PTE), Cottonseed Methyl Ester (CSE), Corn Methyl Ester (CNE), Sunflower Methyl Ester (SNE), Tung Methyl Ester (TGE), Hemp-oil Methyl Ester, produced from Hemp seed oil in Ukraine (HME1), Soybean Methyl Ester (SME), Linseed Methyl Ester (LNE), Hemp-oil Methyl Ester, produced in European Union (HME2), Canola seed Methyl Ester (CAN), Waste cooking-oil Methyl Ester (WME) and Rapeseed Methyl Ester (RME).

It is pointed out that the third model under-predicts the droplet evaporation times compared with the first model (believed to be the most reliable one) by up to about 26%. This result does not support our earlier finding, based on the analysis of only five types of biodiesel fuel in different engine conditions, that the deviations between the evaporation times predicted by these models do not exceed about 5.5%. The evaporation times predicted by the second model have been shown to be reasonably close to those predicted by the first model. The second model under-predicts this time by not more than 4.3% except for Rapeseed Methyl Ester (RME) for which this under-predictions reaches 15.1%. The predictions of the fourth model have been shown to be closer to the predictions of the first model than those of the third model.

As in the case of Diesel and gasoline droplets, for biodiesel droplets the multi-component model predicts higher droplet surface temperatures at the final stages of evaporation (in most cases) and longer evaporation times than the single component model. This is related to the fact that at the final stages of droplet evaporation the mass fraction of heavier species, which evaporate more slowly than the lighter species and have higher boiling temperatures, increases at the expense of lighter species.

Acknowledgments

The authors are grateful to Paul Harris for useful discussions, and INTERREG IVA (Project E3C3, Reference 4274) and the EPSRC (United Kingdom) (Grant EP/K020528/1) for their financial support of the work on this project.

References

- [1] Lapuerta M, Armas O, Rodrigues-Fernandez J. Effect of biodiesel fuels on diesel engine emissions. *Prog Energy Combust Sci* 2008;34:198–223. <http://dx.doi.org/10.1016/j.pecs.2007.07.001>.
- [2] Hoekman SK, Broch A, Robbins C, Cenicerio E, Natarajan M. Review of biodiesel composition, properties, and specifications. *Renew Sustain Energy Rev* 2012;16:143–69. <http://dx.doi.org/10.1016/j.rser.2011.07.143>.
- [3] Al Qubeissi M, Kolodnytska R, Sazhin SS. Biodiesel fuel droplets: modelling of heating and evaporation processes. In: 25th Eur. conf. liq. at. spray syst., Crete, Greece; 2013. Paper No. 4 (CD).
- [4] Kolodnytska R, Al Qubeissi M, Sazhin SS. Biodiesel fuel droplets: transport and thermodynamic properties. In: 25th Eur. conf. liq. at. spray syst., Crete, Greece; 2013. Paper No. 7 (CD).
- [5] Meher LC, Vidya Sagar D, Naik SN. Technical aspects of biodiesel production by transesterification – a review. *Renew Sustain Energy Rev* 2006;10:248–68. <http://dx.doi.org/10.1016/j.rser.2004.09.002>.
- [6] Dunn RO. Cold-flow properties of soybean oil fatty acid monoalkyl ester admixtures. *Energy Fuels* 2009;23:4082–91. <http://dx.doi.org/10.1021/ef9002582>.
- [7] Hill J, Nelson E, Tilman D, Polasky S, Tiffany D. Environmental, economic, and energetic costs and benefits of biodiesel and ethanol biofuels. *Proc Natl Acad Sci* 2006;103:11206–10. <http://dx.doi.org/10.1073/pnas.0604600103>.
- [8] Pan K-L, Li J-W, Chen C-P, Wang C-H. On droplet combustion of biodiesel fuel mixed with diesel/alkanes in microgravity condition. *Combust Flame* 2009;156:1926–36. <http://dx.doi.org/10.1016/j.combustflame.2009.07.020>.
- [9] Tickell J, Roman K. From the fryer to the fuel tank: the complete guide to using vegetable oil as an alternative fuel. New Orleans, LA: Joshua Tickell Media Productions; 2003.
- [10] EPA U. US Environmental Protection Agency n.d. <<http://www.epa.gov/>> (accessed on 15.11.14).
- [11] Yuan W, Hansen AC, Zhang Q. Predicting the physical properties of biodiesel for combustion modeling. *Trans ASAE* 2003;46:1487–93. <http://dx.doi.org/10.13031/2013.15631>.
- [12] Sazhin SS. *Droplets and sprays*. Springer 2014.
- [13] Sanford SD, White JM, Shah PS, Wee C, Valverde MA, Meier GR. Feed Stock and Biodiesel Characteristics Report. Ames, Iowa, USA: Renewable Energy Group; 2009.
- [14] van Gerpen J. Biodiesel processing and production. *Fuel Process Technol* 2005;86:1097–107. <http://dx.doi.org/10.1016/j.fuproc.2004.11.005>.
- [15] Knothe G. Biodiesel and renewable diesel: a comparison. *Prog Energy Combust Sci* 2010;36:364–73. <http://dx.doi.org/10.1016/j.pecs.2009.11.004>.
- [16] Grabar IG, Kolodnytska RV, Semenov VG. Biofuel based on oil for diesel engines. Zhytomyr: ZDTU; 2011 (in Ukrainian).
- [17] Sazhin SS, Al Qubeissi M, Nasiri R, Gunko VM, Elwardany AE, Lemoine F, et al. A multi-dimensional quasi-discrete model for the analysis of Diesel fuel droplet heating and evaporation. *Fuel* 2014;129:238–66. <http://dx.doi.org/10.1016/j.fuel.2014.03.028>.
- [18] Sazhin SS, Al Qubeissi M, Kolodnytska R, Elwardany AE, Nasiri R, Heikal MR. Modelling of biodiesel fuel droplet heating and evaporation. *Fuel* 2014;115:559–72. <http://dx.doi.org/10.1016/j.fuel.2013.07.031>.
- [19] Sazhin SS, Al Qubeissi M, Heikal MR. Modelling of biodiesel and diesel fuel droplet heating and evaporation. In: 15th int. heat transf. conf. IHTC-15, paper Begellhouse IHTC15-8936; 2014. <http://dx.doi.org/10.1615/IHTC15.evp.008936>.
- [20] Mata TM, Cardoso N, Ornelas M, Neves S, Caetano NS. Sustainable production of biodiesel from tallow, lard and poultry fat and its quality evaluation. *Chem Eng Trans* 2010;19:13–8. <http://dx.doi.org/10.3303/CET1019003>.
- [21] Dirbude S, Eswaran V, Kushari A. Droplet vaporization modeling of rapeseed and sunflower methyl esters. *Fuel* 2012;92:171–9. <http://dx.doi.org/10.1016/j.fuel.2011.07.030>.
- [22] Tyson KS, Bozell J, Wallace R, Petersen E, Moens L. Biomass oil analysis: research needs and recommendations. National Renewable Energy Lab., Golden, CO (USA); 2004. doi: <http://dx.doi.org/10.2172/15009676>.
- [23] Park J-Y, Kim D-K, Wang Z-M, Lu P, Park S-C, Lee J-S. Production and characterization of biodiesel from tung oil. *Appl Biochem Biotechnol* 2008;148:109–17. <http://dx.doi.org/10.1007/s12010-007-8082-2>.
- [24] Giakoumis EG. A statistical investigation of biodiesel physical and chemical properties, and their correlation with the degree of unsaturation. *Renew Energy* 2013;50:858–78. <http://dx.doi.org/10.1016/j.renene.2012.07.040>.
- [25] Hopfe D. Thermophysical data of pure substances. in: Data Compilation of FIZ CHEMIE, Germany; 1990. p. 20.
- [26] Kolodnytska RV. Analytical study for atomization of hemp oil biodiesel. *Visnik East-Ukr Natl Univ* 2010;6:416.
- [27] NIST. Natl. Inst. Stand. Technol.; 2014. <<http://webbook.nist.gov/chemistry/fluid/>> (accessed on 28.02.14).

- [28] Park SH, Kim HJ, Suh HK, Lee CS. Experimental and numerical analysis of spray-atomization characteristics of biodiesel fuel in various fuel and ambient temperatures conditions. *Int J Heat Fluid Flow* 2009;30:960–70. <http://dx.doi.org/10.1016/j.ijheatfluidflow.2009.04.003>.
- [29] Dos Santos F, Le Moyne L. Spray atomization models in engine applications, from correlations to direct numerical simulations. *Oil Gas Sci Technol – Rev D'IFP Energ Nouv* 2011;66:801–22. <http://dx.doi.org/10.2516/ogst/2011116>.
- [30] Choi S, Oh Y. The spray characteristics of unrefined biodiesel. *Renew Energy* 2012;42:136–9. <http://dx.doi.org/10.1016/j.renene.2011.08.047>.
- [31] Pandey RK, Rehman A, Sarviya RM. Impact of alternative fuel properties on fuel spray behavior and atomization. *Renew Sustain Energy Rev* 2012;16:1762–78. <http://dx.doi.org/10.1016/j.rser.2011.11.010>.
- [32] Crua C, de Sercey G, Gold M, Heikal MR. Image-based analysis of evaporating diesel sprays in the near-nozzle region. In: 25th Eur. conf. liq. at. spray syst. Chania, Greece; 2013.
- [33] Al Qubeissi M, Sazhin SS, de Sercey G, Crua C. Multi-dimensional quasi-discrete model for the investigation of heating and evaporation of Diesel fuel droplets. In: 26th Eur. conf. liq. at. spray syst., CD, paper ABS-135, Bremen, Germany: University of Bremen; 2014.
- [34] Arias-Zugasti M, Rosner DF. Multicomponent fuel droplet vaporization and combustion using spectral theory for a continuous mixture. *Combust Flame* 2003;135:271–84. [http://dx.doi.org/10.1016/S0010-2180\(03\)00166-4](http://dx.doi.org/10.1016/S0010-2180(03)00166-4).
- [35] Abdel-Qader Z, Hallett WLH. The role of liquid mixing in evaporation of complex multicomponent mixtures: modelling using continuous thermodynamics. *Chem Eng Sci* 2005;60:1629–40. <http://dx.doi.org/10.1016/j.ces.2004.10.015>.
- [36] Rivard E, Brüggemann D. Numerical investigation of semi-continuous mixture droplet vaporization. *Chem Eng Sci* 2010;65:5137–45. <http://dx.doi.org/10.1016/j.ces.2010.06.010>.
- [37] Burger M, Schmehl R, Prommersberger K, Schäfer O, Koch R, Wittig S. Droplet evaporation modeling by the distillation curve model: accounting for kerosene fuel and elevated pressures. *Int J Heat Mass Transfer* 2003;46:4403–12. [http://dx.doi.org/10.1016/S0017-9310\(03\)00286-2](http://dx.doi.org/10.1016/S0017-9310(03)00286-2).
- [38] Zhang L, Kong S-C. Vaporization modeling of petroleum-biofuel drops using a hybrid multi-component approach. *Combust Flame* 2010;157:2165–74. <http://dx.doi.org/10.1016/j.combustflame.2010.05.011>.
- [39] Laurent C, Lavergne G, Villedieu P. Continuous thermodynamics for droplet vaporization: comparison between Gamma-PDF model and QMoM. *CR Mécanique* 2009;337:449–57.
- [40] Sazhin SS, Krutitskii PA, Gusev IG, Heikal M. Transient heating of an evaporating droplet with presumed time evolution of its radius. *Int J Heat Mass Transfer* 2011;54(5–6):1278–88. <http://dx.doi.org/10.1016/j.ijheatmasstransfer.2010.10.018>.